COVERS WP4 Benchmark 1

Fracture mechanical analysis of a thermal shock scenario for a VVER-440 RPV

Martin Abendroth; Eberhard Altstadt

Juni 2007

WISSENSCHAFTLICH-TECHNISCHE BERICHTE

Forschungszentrum Dresden Rossendorf

COVERS WP4 Benchmark 1

Fracture mechanical analysis of a thermal shock scenario for a VVER-440 RPV

Authors:

Martin Abendroth
Eberhard Altstadt

June 04, 2007

Abstract

This paper describes the analytical work done by modelling and evaluating a thermal shock in a WWER-440 reactor pressure vessel due to an emergency case. An axial oriented semi-elliptical underclad/surface crack is assumed to be located in the core weld line. Three-dimensional finite element models are used to compute the global transient temperature and stress-strain fields. By using a three-dimensional submodel, which includes the crack, the local crack stress-strain field is obtained. With a subsequent postprocessing using the j-integral technique the stress intensity factors K_I along the crack front are obtained. The results for the underclad and surface crack are provided and compared, together with a critical discussion of the VERLIFE code.

Contents

1   Introduction

The presented work is part of a benchmark from the workpackage four of the COVERS project [1] within the Sixth Framework Programme of EURATOM. Aim of the COVERS project is to '...*establish a viable research and technical development structure with a view to change the scientific and technical cooperation of actors involved in WWER safety research, in close co-operation with utilities, manufacturers, regulatory bodies and other end users.*'

One important point of workpackage four with the title '*Material and Equipment Ageing*' is '...*to test and update the existing common unified procedure on plant life assessment VERLIFE. This document is prepared within FP5 with limited experience of practical use. It should be revised based on the:*

- *Available new information*

- *Experience gained during practical use*

- *Benchmark tests of different factors affecting the calculated service life according to VERLIFE*'

The benchmark discussed here, refers to the chapter 5 of the VERLIFE code [6], which defines the assessment of component resistance against fast fracture. This assessment is based on the stress intensity factors K_I for a postulated crack. Especially, the code recommends the j-integral to obtain the stress intensity factors. The well known j-integral introduced by Eshelby [8], Cherepanov [7] and Rice [11] and modified by Shih at al. [12] is a measure for crack loading and directly related to the stress intensity factors. It has been used by Bass at al. [3, 4], Kikuchi at al. [9] and Sievers and Höfler [13] to evaluate cracks in thermo-mechanical loaded pressure vessels.

2   Benchmark Definition

The given scenario describes a pressurized thermal shock (PTS) regime for a reactor pressure vessel (RPV) of the type WWER-440/V-213. The main reactor cooling system has failed and the emergency cooling system is the only source of cooling fluid. Additionally, an unintentional opening of a pressurizer safety valve (PRZ SV) is assumed, which will be closed again after 3600 seconds. This scenario results in two opposite cold plumes below the cold legs in the downcomer of the RPV, which suddenly cool the inside of the RPV. The undercooled region includes the core weld line, which is supposed to be one of the most embrittled regions of the RPV due to neutron radiation. Additionally, weld lines are also likely locations for cracks or flaws. Therefore, the scenario postulates an axial oriented semi-elliptical underclad crack. The axial orientation is chosen because of the maximum principal stress in a pressurized cylindric vessel is acting in hoop direction and so perpendicular to the faces of the postulated crack. The undercooled inner surface of the RPV and the crack are exposed to tensile stress. Repressurizing the RPV after 3600 seconds by closing the safety valve will suddenly increase the tensile stress and is assumed to be the critical phase of the scenario.

The primary questions regarding this scenario are:

- What is the loading of the crack during this scenario?

- What are the stress intensity factors during this scenario?

- What are the allowable stress intensity factors based on critical temperatures of brittleness T_k?

- What is the allowable critical temperature T_k^a of the material?

2.1   Detailed description of the problem

The component of interest is a WWER-440/V-213 RPV, which has an inner radius of $r_i = 1771\,\text{mm}$. The inner surface has a cladding with a thickness of $s_{\text{clad}} = 9\,\text{mm}$. The thickness of the base material in the cylindric part of the vessel is $s_{\text{base}} = 140\,\text{mm}$. The geometry of the two opposite cold plumes is given by means of levels, whereas level means the vertical distance below the lower part of the cold leg (see Fig. 3). Table 1 shows the figures of the cold plumes. The geometry and the physical properties of the cold plume were obtained from a thermohydraulic simulation, which is not part of this benchmark [10].

There is zero heat transfer at the outside of the vessel, which is reasonable because of the existence of an outer thermal isolation. The stress free temperature of the cladded vessel is $T_{sf} = 267\,^\circ\text{C}$. The weld material has the same thermal-physical and tensile properties as the base material but is supposed to have residual stresses σ_R in both axial and circumferential orientation. These residual stresses result from the welding process.

$$\sigma_R = 60\,\text{MPa} \cdot \cos\left(\frac{2\pi x}{s_{\text{base}}}\right) \tag{1}$$

Here, x is the radial coordinate starting from the interface of cladding and base material to the outside of the vessel. The postulated semi-elliptical underclad crack is located at

the core weld 5/6 at level 3.485 m. As already mentioned above, this weld accumulates the highest damage (embrittlement) due to neutron radiation of all welds from the RPV and is therefore the most critical one, which means that the ductile to brittle transition temperature (DBTT) for this weld line is above the DBTT for all the others.

The supposed crack width is $a = 15\,\text{mm}$ and the width/length ratio is $a/c = 0.3$. The crack is orientated in axial direction. The temperature dependent allowable stress intensity is given according to the VERLIFE code [6] Chapter 5.6 as:

$$[K_{IC}]_3 = 26 + 36\exp[0.02\,(T - T_k)] \qquad (2)$$

with $[K_{IC}]_{3max} = 200\,\text{MPam}^{0.5}$. T denotes the temperature at the crack tip and T_k the critical temperature, obtained from the ductile-to-brittle transition temperature.

The tables 2 and 3 give the thermal-physical and tensile properties for the irradiated state of the base and the cladding material. In table 4 the heat transfer coefficient of the cold plum and the ambient region in the downcomer are given. Fig. 1 shows the internal pressure changing in time due to the opening and reclosure of the PRZ SV. In Fig. 2 the coolant temperature in the downcomer is plotted over the time for the different levels.

Table 1: Cold plume geometry

level [m]	width [m]
0.000	0.8
0.785	0.8
3.485	1.8
> 3.485	1.8

Table 2: Thermal-physical properties of base and weld material [6], App. XV, T – temperature, E – elastic modulus, α_{ref}, α_0 – thermal expansion coefficient based on reference and absolute temperature, ν – Poisson ratio, λ – thermal conductivity, c_p – specific heat, ρ – density
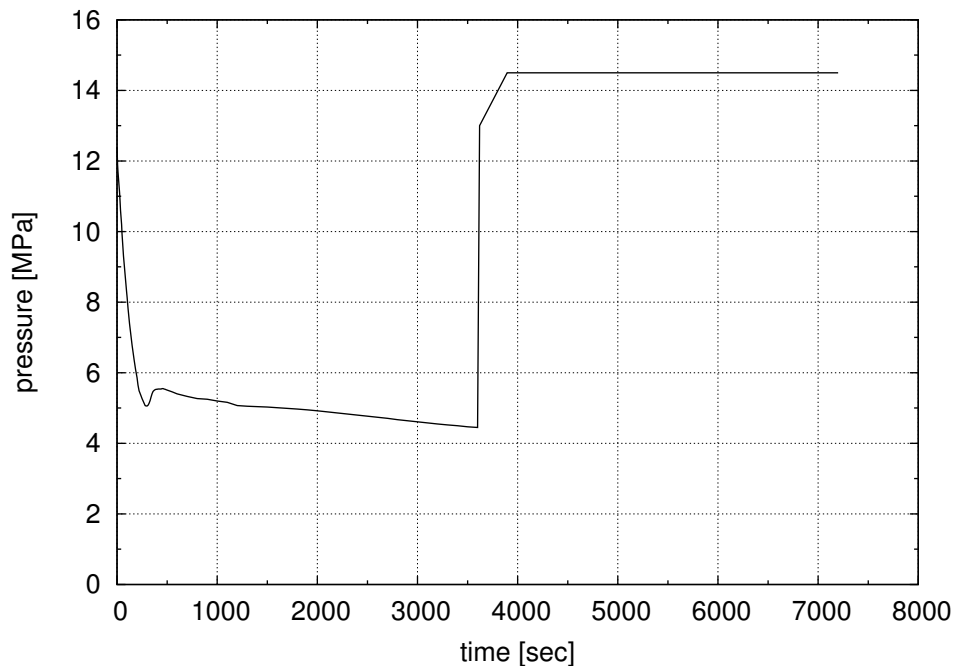
| mat. | T | E | α_{ref} | α_0 | ν | λ | c_p | ρ |
	[°C]	[GPa]	[$10^{-6}\,\text{K}$]		[-]	$\left[\frac{\text{W}}{\text{m}\,\text{K}}\right]$	$\left[\frac{\text{J}}{\text{kg}\,\text{K}}\right]$	$\left[\frac{\text{kg}}{\text{m}^3}\right]$
base	20	210	-	12.9	0.3	35.9	445	7821
and	100	205	11.9	13.3	0.3	37.3	477	7799
weld	200	200	12.5	13.9	0.3	38.1	520	7771
	300	195	13.1	14.5	0.3	37.3	562	7740
clad	20	165	-	15.9	0.3	15.1	461	7900
	100	160	14.6	16.5	0.3	16.3	494	7868
	200	153	15.7	16.5	0.3	17.6	515	7830
	300	146	16.0	16.8	0.3	18.8	536	7790

Table 3: Tensile properties for the irradiated state of base and weld material

material	T	$R_{P0.2}$	E_T
	[°C]	[MPa]	[MPa]
base/	20	625	870
weld	300	555	870
clad	20	426	876
	300	326	676

Table 4: Heat transfer coefficient in the downcomer

time	cold plume	ambient
[sec]	[Wm^{-2}K^{-1}]	[Wm^{-2}K^{-1}]
0	10000	10000
420	10000	10000
440	5000	1800
3650	5000	1800
3651	1000	1000
7200	1000	1000

Figure 1: Internal pressure, PRZ SV inadvertent opening with reclosure at 3600 seconds.
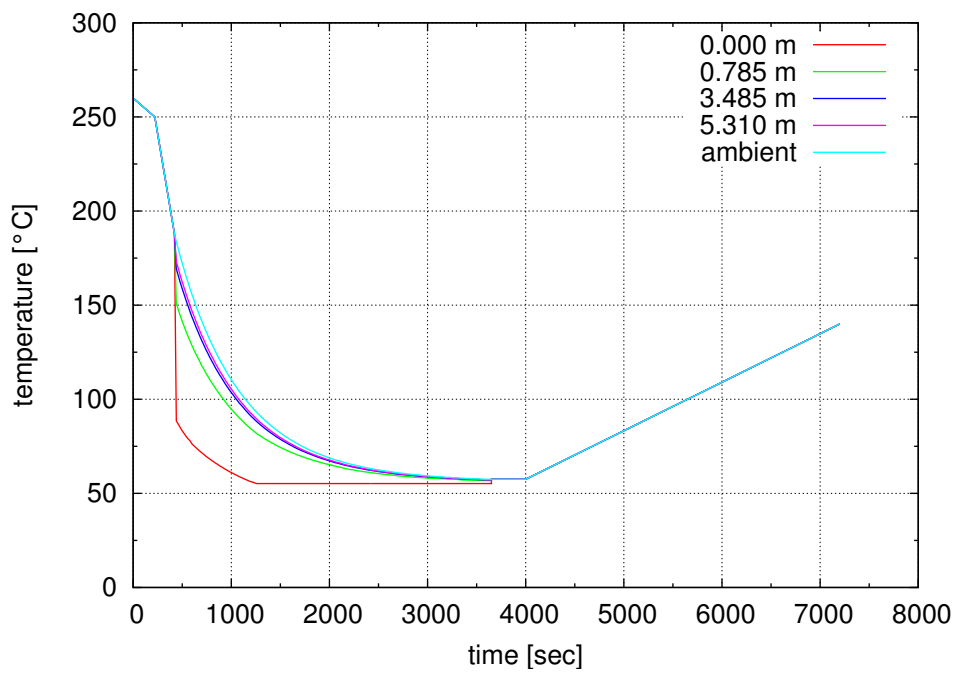
Figure 2: Coolant temperature in the cold plumes and the ambient region in the downcomer.

3   Numerical Methods

3.1   Geometric Modelling

To solve the given problem we use a three-dimensional finite element (FE) model of one quarter of the RPV. Since the region of interest (core weld 5/6) is far away from the in- and outlets, these nozzles have been neglected in the model. This model does not contain any crack so far. It is used to compute in a first run the transient spatial thermal field.

Fig. 3 shows the computed thermal field at the time $t = 1000\,\mathrm{s}$. On the right part of the figure the cold plume is clearly to see. The incoming cold water leads to a general cool down of the inner surface of the RPV, but especially in the cold plum region the temperatures are up to $50\,\mathrm{K}$ lower than in the ambient region. This leads to elevated tensile stresses in hoop and vertical direction in the cold plum region of the inner surface of the RPV.

In a second run the mechanical solution is obtained using the thermal field as a body load. In the mechanical solution also the time dependent inner pressure, the acceleration of gravity and the initial residual stresses in the welds are considered.

Fig. 4 shows the computed hoop stress at the time $t = 1000\,\mathrm{s}$. It can be seen that in general the highest hoop stresses are located in the cladding which is directly in contact with the coolant. Secondly, we identify the upper part, where the vessel wall thickness is greater than in the lower part, having in general higher hoop stress values than the lower part. And thirdly, the cold plum region in the lower part is also a region with elevated hoop stress.

In Fig. 5 the cladding is virtually removed and we have a direct view to the base and weld material. It can be seen that the weld lines have higher hoop stress values than the base material. This is due to the residual stresses, which are applied before the simulation starts. With a closer look we find that the upper weld lines are subjected to higher hoop stresses, the reason for this is the greater RPV wall thickness. But we have to keep in mind that the upper weld lines are much less damaged due to radiation than the core weld line.

To consider cracks in the model we use a submodel technique. Two different crack are assumed, a underclad crack as defined in the benchmark and a surface crack as shown in Fig. 6. Only the crack and a reasonable large surrounding is modeled. At the cut boundaries of the submodel the interpolated degree of freedom results (displacements) of the global (coarse) model are applied. The thermal field obtained in the first run and the gravity loads are used as a body loads. Additionally, the pressure (see Fig. 1) is applied at the inner surface. Fig. 8 shows the equivalent stress in the submodel at time $t = 1000$ seconds. The crack is assumed to be an underclad crack. Here arises a principal problem, since the cladding itself contains no crack and has common nodes with the base material, the crack mouth is virtually clamped close, which results in a second straight and sharp crackfront at the interface between cladding and base material.

The VERLIFE code does make any suggestions how to deal numerically with underclad cracks. Therefore a second submodel is used, which includes a surface crack which goes through the cladding. Fig. 9 shows the hoop stress at $t = 1000\,\mathrm{s}$. Here, the crack face is clearly distinguishable from the rest of the model.
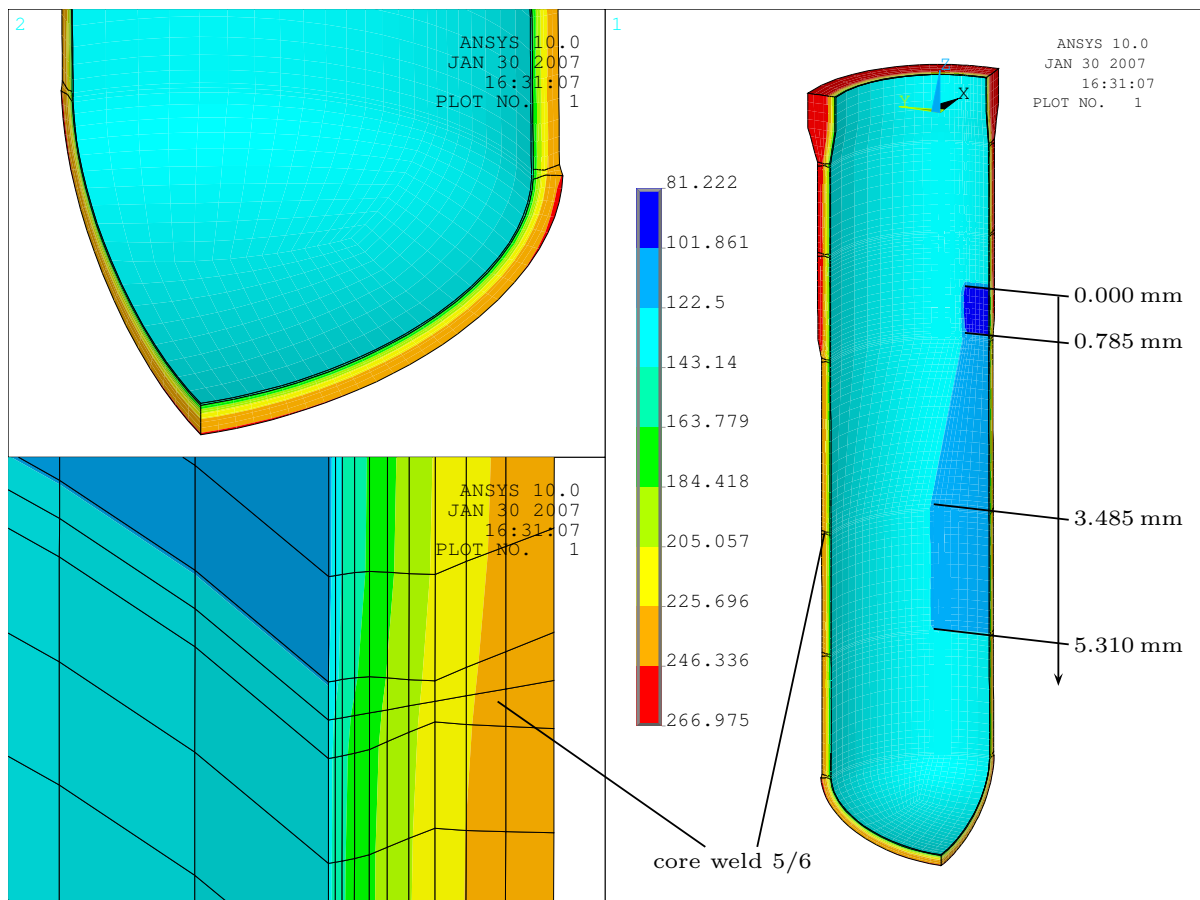
Figure 3: Temperature [°C] after 1000 seconds; Right: whole model; Top left: detail of the RPV bottom; Bottom left: detail of the weld line 5/6
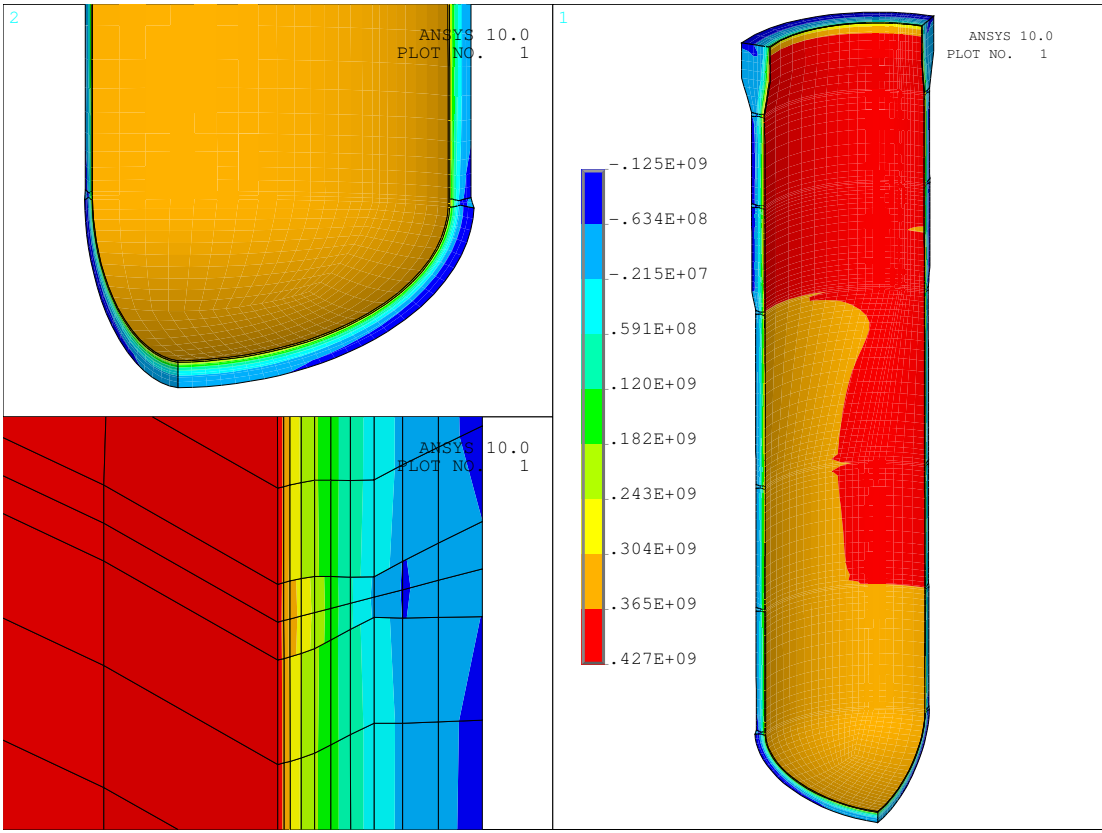
Figure 4: Hoop stress [Pa] after 1000 seconds; Right: whole model; Top left: detail of the RPV bottom; Bottom left: detail of the weld line 5/6
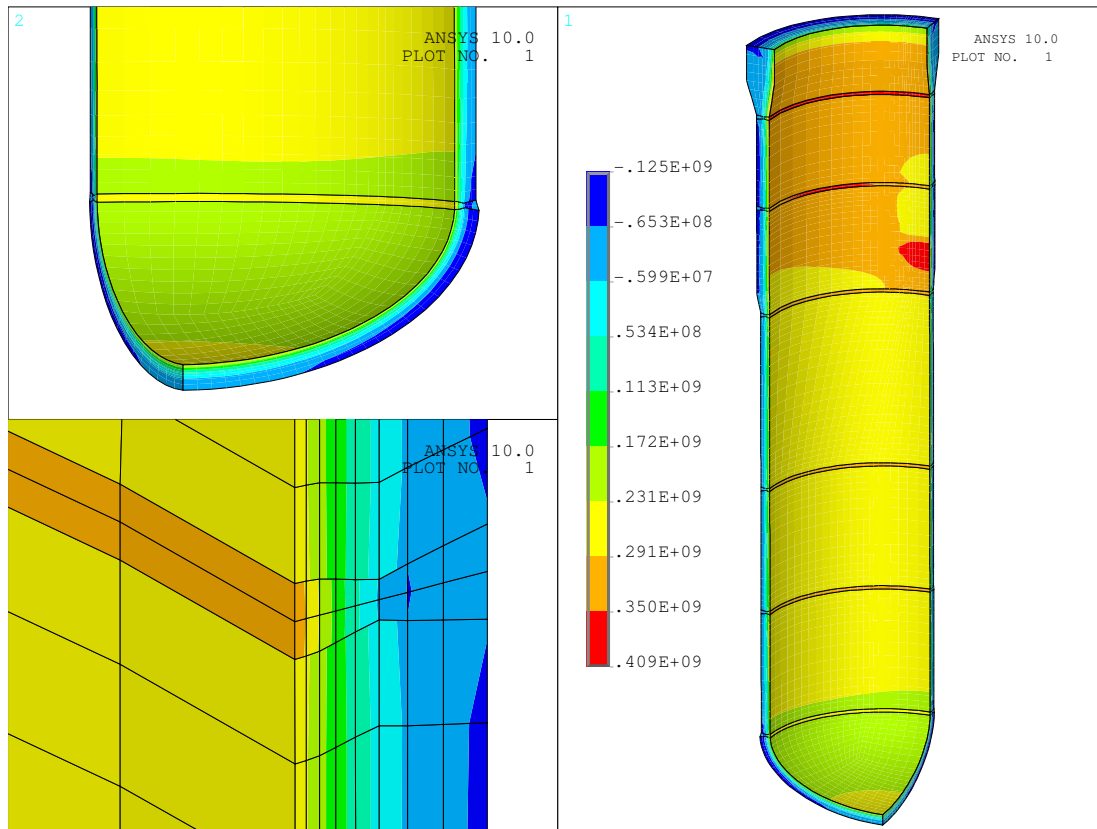
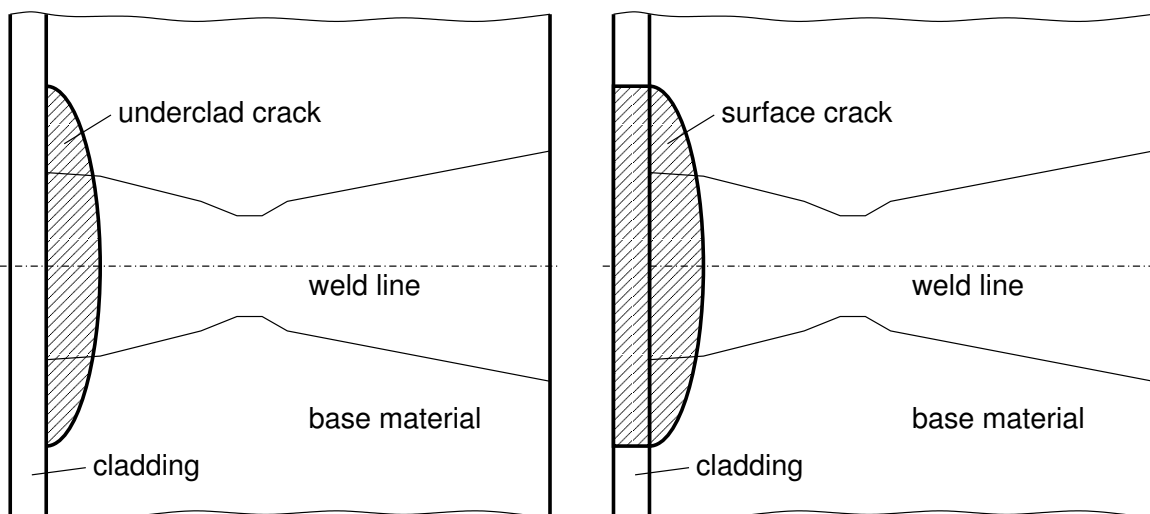**Figure 5:** Hoop stress [Pa] (no cladding) after 1000 seconds; Right: whole model; Top left: detail of the RPV bottom; Bottom left: detail of the weld line 5/6

Figure 6: Geometry of the underclad and surface crack
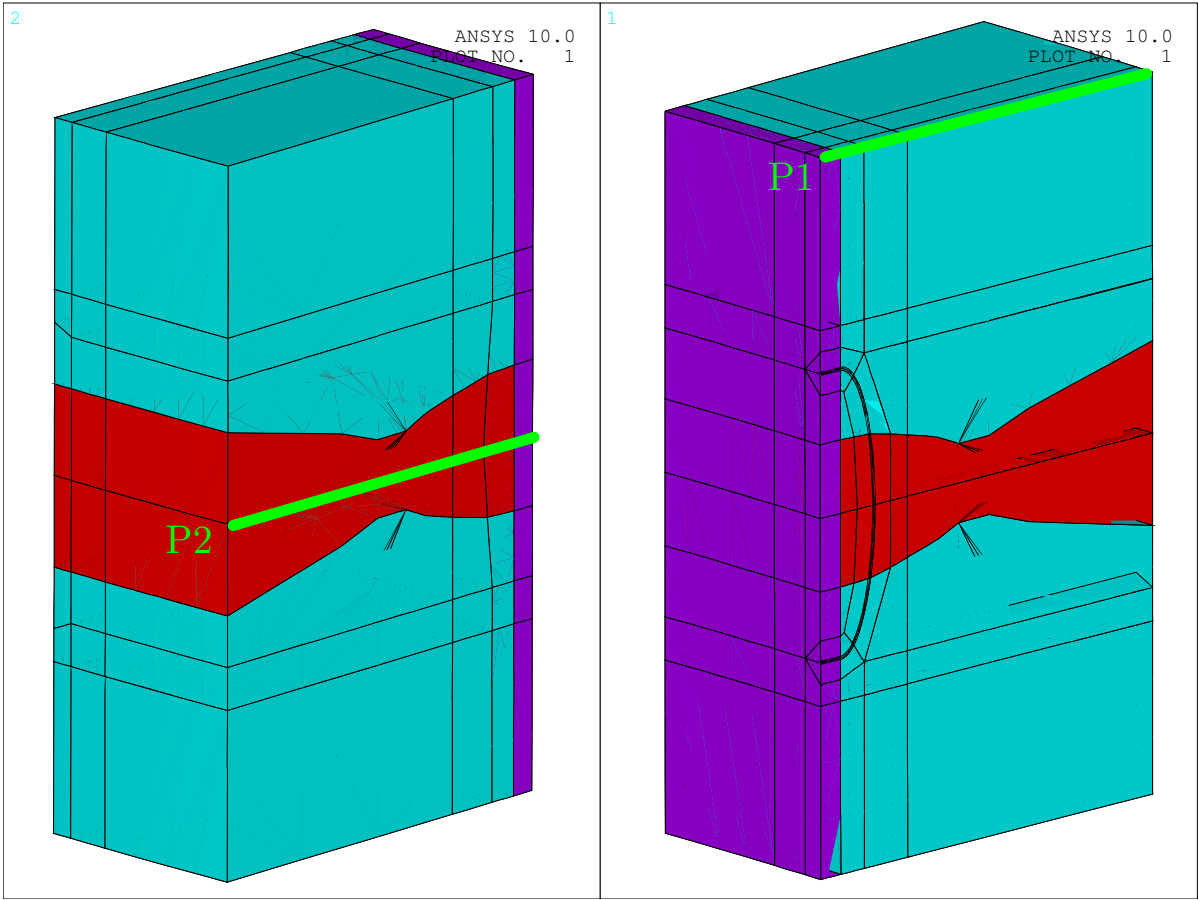
Figure 7: Volume plot of the underclad submodel, different colors indicate different materials, blue - base material, red - weld material, magenta - cladding, green - path definitions
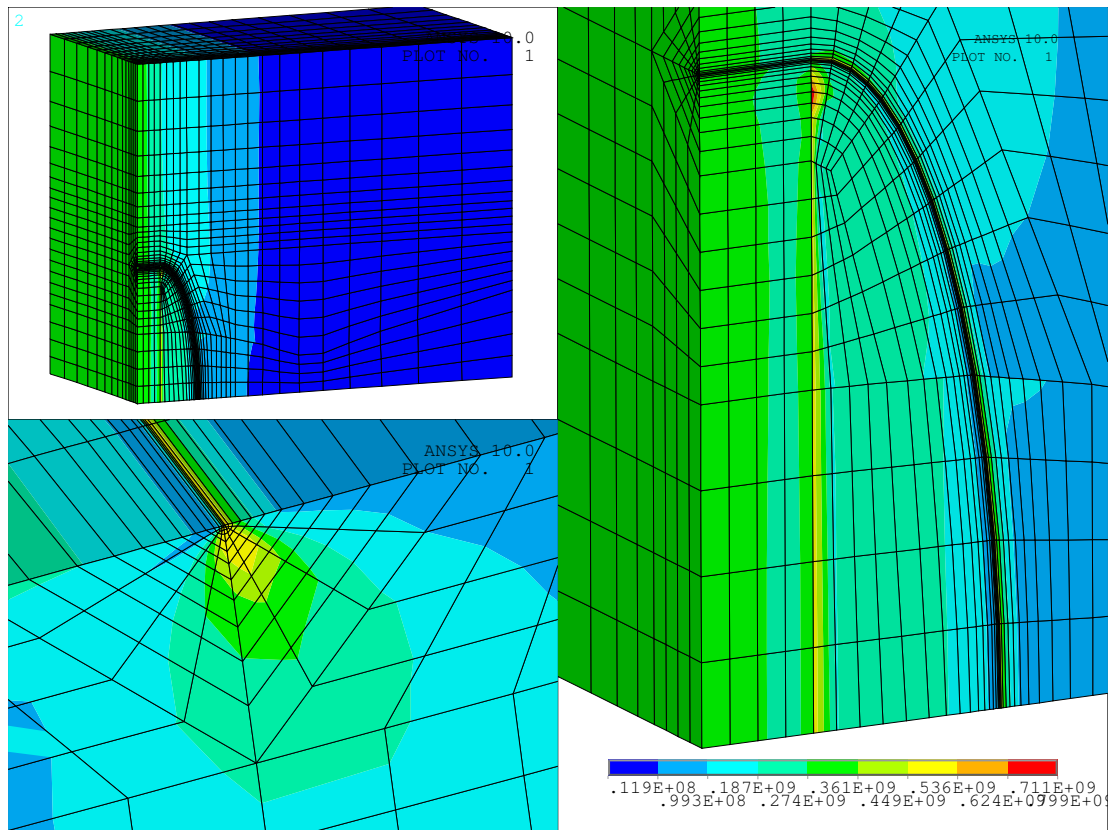
Figure 8: Equivalent stress [Pa] for the underclad submodel after 1000 seconds, top left) upper half of the submodel, bottom left) view on the crack tip, right) crack in detail of the upper half of the submodel
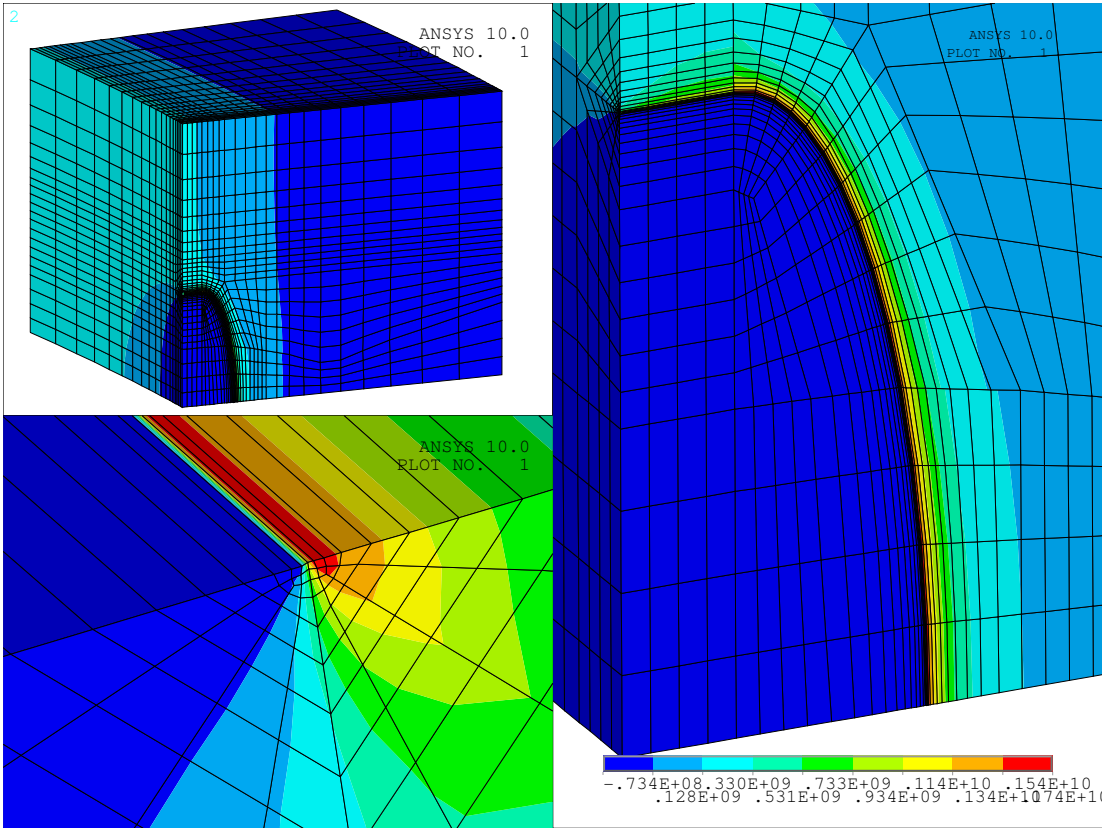
Figure 9: Hoop stress [Pa] for the surface crack submodel after 1000 seconds, top left) upper half of the submodel, bottom left) view on the crack tip, right) crack in detail of the upper half of the submodel

3.2   Submodel verification

The submodels need to be verified. The stresses on the cut boundaries of the submodel shall have the same values as the stresses in the global model at the same locations. To evaluate these stresses two paths have been defined, as can be seen in Fig. 7. Path P1 is located at the upper cut boundary in the same plane as the crack. Path P2 is defined at the cut boundary in positive hoop direction at the hight of the deepest crack point.

The Figures 10 - 13 show an acceptable agreement between the global and submodel stresses for both paths and both crack models. The submodel for the surface crack has the double arc length in hoop direction than the underclad crack submodel, to obtain an acceptable accuracy.
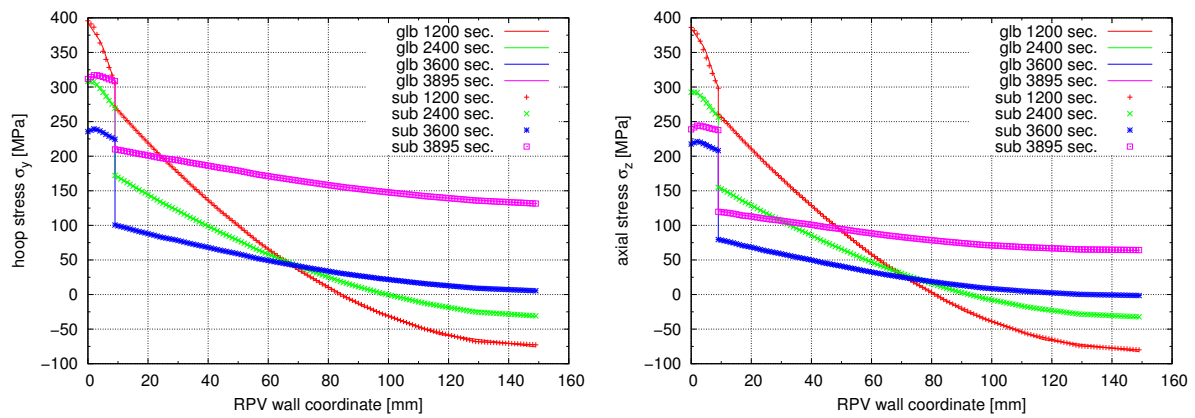

Figure 10: Comparison of hoop and axial stress obtained from the global and the submodel for path 1 for the underclad crack submodel
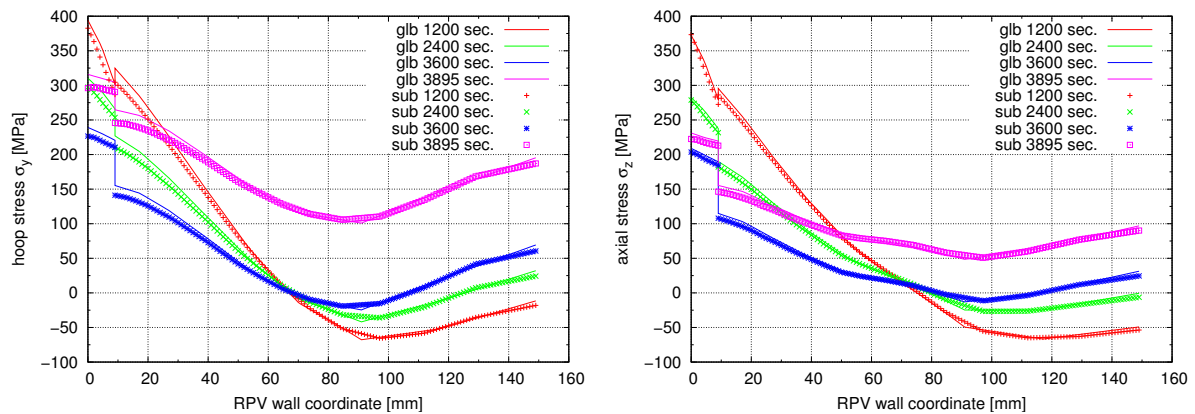

Figure 11: Comparison of hoop and axial stress obtained from the global and the submodel for path 2 for the underclad crack submodel
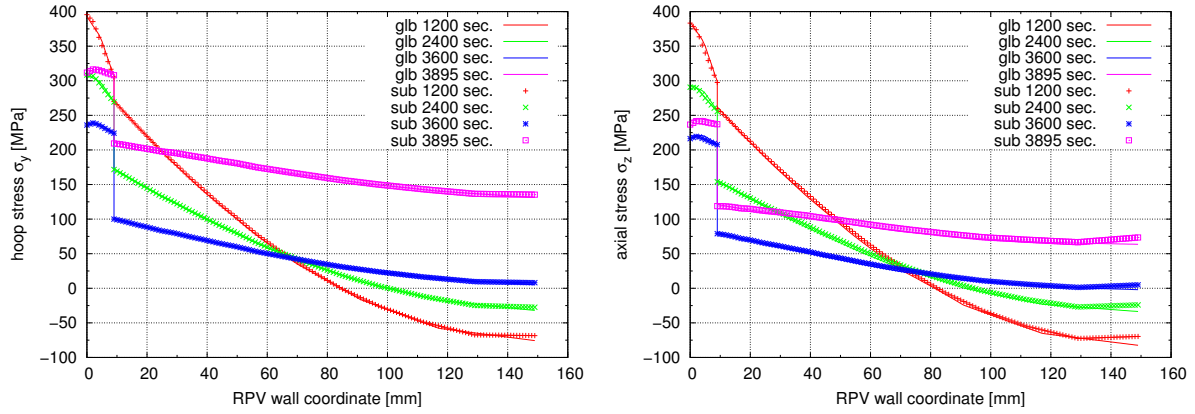
Figure 12: Comparison of hoop and axial stress obtained from the global and the submodel for path 1 for the surface crack submodel
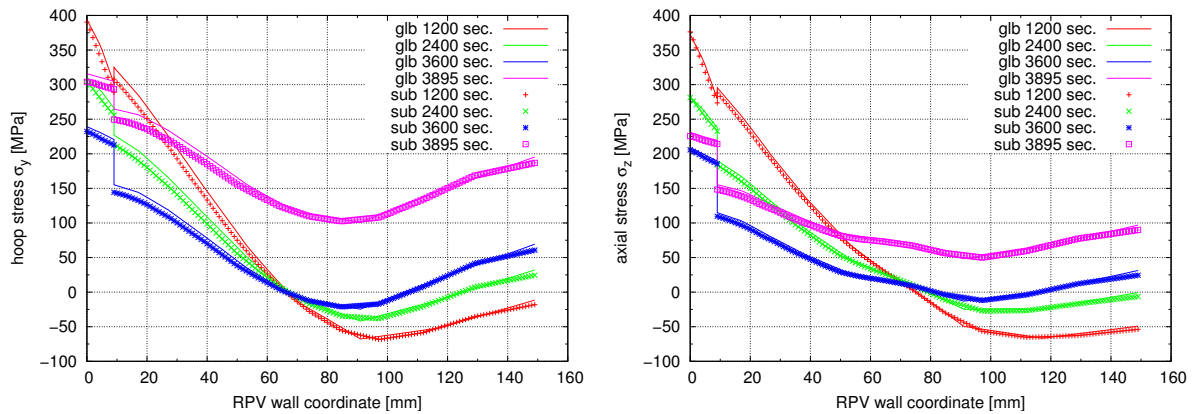

Figure 13: Comparison of hoop and axial stress obtained from the global and the submodel for path 2 for the surface crack submodel

3.3   Computation of stress intensity factors

For a crack loaded in mode I the stress intensity factor K_I is related to the first component of the j-integral J_1. For a plane strain state the relation is

$$K_I = \sqrt{\frac{J_1 E}{1 - \nu^2}} \tag{3}$$

and for a plane stress state

$$K_I = \sqrt{J_1 E}. \tag{4}$$

Here, E denotes the elastic modulus and ν Poisson's ratio of the material.

3.3.1   The ANSYS kcalc method

A different approach is used by the ANSYS FE-code for elastic problems:

$$K_I = \sqrt{2\pi} \frac{2G}{1 + \kappa} \frac{|u_y|}{\sqrt{r}}, \tag{5}$$

with the shear modulus G and stress state dependent κ

$$G = \frac{E}{2(1 + \nu)}, \quad \kappa = 3 - 4\nu \quad \text{and} \quad \kappa = \frac{3\nu}{1 + \nu} \tag{6}$$

for plane strain and plane stress respectively. $|u_y|$ denotes the displacements perpendicular to the crack face for a model, which is symmetric to the ligament. r is the radial distance from the crack tip. Three pairs of $|u_y|$ and r are determined at node A located at the crack tip, and two nodes B and C, which are located at the crack face. The displacements are normalized so that $|u_y|$ at node A is zero. Then two constants c_1 and c_2 are determined so that

$$\frac{|u_y|}{\sqrt{r}} = c_1 + c_2 r \tag{7}$$

at the nodes B and C. Then, let r approach 0

$$\lim_{r \to 0} \frac{|u_y|}{\sqrt{r}} = c_1 \tag{8}$$

and Eq. 5 becomes

$$K_I = \sqrt{2\pi} \frac{2G}{1 + \kappa} c_1. \tag{9}$$

The distances from the crack tip of the nodes B and C used to obtain $|u_y|$ are $3.75\,\text{mm}$ and $7.5\,\text{mm}$ for the underclad crack model and $7.5\,\text{mm}$ and $15\,\text{mm}$ for the surface crack model.

3.3.2 The VERLIFE method

The VERLIFE code gives a deterministic formula to estimate the stress intensity factor.

$$K_I = \sigma_k Y \sqrt{a} \tag{10}$$

This relation is also valid only for linear elastic cases. Here, σ_k is an effective stress measure obtained from the through wall distribution of the stress components normal to the postulated crack face. For a surface crack the effective stress is

$$
\begin{aligned}
\sigma_k &= 0.111 \left(3\sigma_A + \sigma_B + 5\sigma_c\right) \\
&+ 0.4\frac{a}{c}\left(0.38\sigma_A - 0.17\sigma_B - 0.21\sigma_C\right) \\
&- 0.28\frac{a}{s}\left(1 - \sqrt{\frac{a}{c}}\right)\left(\sigma_A - \sigma_B\right)
\end{aligned}
\tag{11}
$$

and for an underclad crack

$$\sigma_k = \frac{\sigma_A + \sigma_C}{2} + \frac{a}{c} \cdot \frac{4\sigma_A - 3\sigma_C - \sigma_B}{30}. \tag{12}$$

The stress components σ_A, σ_B, and σ_C are calculated for the uncracked wall considering, however, the residual stresses in the weld. Y is a shape factor depending on the crack geometry, which is for a surface crack

$$Y = \frac{2 - 0.82\frac{a}{c}}{\left[1 - \left(0.89 - 0.57\sqrt{\frac{a}{c}}\right)^3 \left(\frac{a}{s}\right)^{1.5}\right]^{3.25}} \tag{13}$$

and for an underclad crack

$$Y = \frac{1.79 - 0.66\frac{a}{c}}{\left[1 - \left(\frac{a}{b+a}\right)^{1.8}\left(1 - 0.4\frac{a}{c} - 0.8\left\{0.5 - \frac{b+a}{s}\right\}^{0.4}\right)\right]^{0.54}}. \tag{14}$$

The following table shows the geometric values, which are used to compute the stress intensity factor according to Eq. 10. The values for A, B and C are the distances from the inner vessel surface for the points where the normal stress components σ_A, σ_B and σ_C are obtained. s denotes the wall thickness, a and c the half crack width and length. Finally for the underclad crack, b is the distance of the point of the crack closest to the nearest surface from this surface, which is the length of the shorter ligament.

Table 5: Geometric values [mm] used to compute the stress intensity factor according to the VERLIFE code

value [mm]	A	B	C	a	c	s	b
underclad crack	24	9	16.5	15	50	149	9
surface crack	24	0	12	24	50	149	-

3.3.3 The j-integral method

For the benchmark we will use the j-integral approach. For a two-dimensional case the first component of the j-integral is

$$J_1 = \int_\Gamma \left(w\delta_{j1} - \sigma_{ij}u_{i,1} \right) n_j d\Gamma. \tag{15}$$

Here, w denotes the strain energy density

$$w = \int_{\varepsilon_{ij}} \sigma_{ij} d\varepsilon_{ij} \tag{16}$$

with the total strain tensor ε_{ij} and the stress tensor σ_{ij}. δ_{ij} is the Kronecker Symbol and $u_{i,1}$ denotes the partial derivative in x(1)-direction of the displacement u_i. Furthermore, the Einstein notation is used, which means that we summarize all terms with double indices over the number of dimensions of the problem. Equation (15) can be extended for to the three-dimensional case. As shown in Fig. 14 we consider a plane crack with an
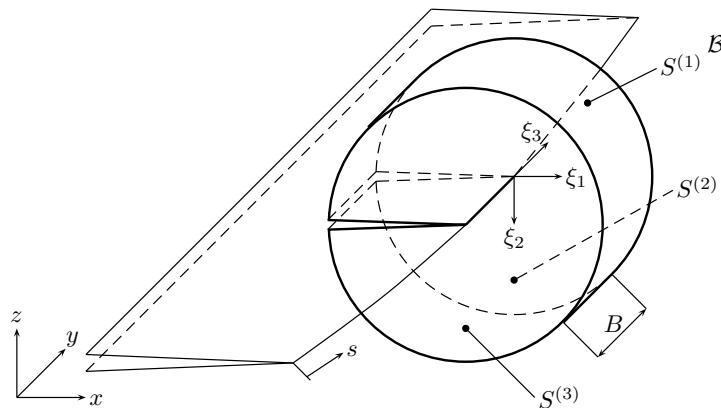

Figure 14: Three dimensional surface integration around a plane crack with arbitrary shaped crack front

arbitrary shaped crack front in a body $\mathcal{B}$. We define a local cartesian coordinate system with the ξ_1-axis pointing in crack extension direction, ξ_2 pointing normal to the plane crack faces and ξ_3 is bound to point in tangential direction of the curved crack front. The integration is now done over the surfaces of a cylindrical volume of the length B, which includes a part of the crack front. $S^{(1)}$ is the cylindrical surface, $S^{(2)}$ and $S^{(3)}$ are the upper and lower bounds of the cylinder. Instead of Eq. (15) we write

$$F_1 = \int_{S^{(1)}+S^{(2)}+S^{(3)}} \left(w\delta_{j1}n_j - \sigma_{ij}n_j u_{i,1} \right) dS. \tag{17}$$

This can be split up into a sum of three separate integrals

$$F_1 = F_1^{S^{(1)}} + F_1^{S^{(3)}} + F_1^{S^{(3)}}, \tag{18}$$

which are

$$F_1^{S^{(1)}} = B \int_\Gamma \left(w\delta_{j1}n_j^\Gamma - \sigma_{ij}n_j^\Gamma u_{i,1} \right) d\Gamma, \tag{19}$$

$$F_1^{S^{(2)}} = \int_{S^{(2)}} \left(w\delta_{j1}n_j^{S^{(2)}} - \sigma_{ij}n_j^{S^{(2)}}u_{i,1} \right) dS^{(2)}, \tag{20}$$

$$F_1^{S^{(3)}} = \int_{S^{(3)}} \left(w\delta_{j1}n_j^{S^{(3)}} - \sigma_{ij}n_j^{S^{(3)}}u_{i,1} \right) dS^{(3)}. \tag{21}$$

The outward normals on the three surfaces are

$$n_j^\Gamma = \begin{bmatrix} n_1^\Gamma \\ n_2^\Gamma \\ 0 \end{bmatrix}, \quad n_j^{S^{(2)}} = \begin{bmatrix} 0 \\ 0 \\ 1 \end{bmatrix}, \quad n_j^{S^{(3)}} = \begin{bmatrix} 0 \\ 0 \\ -1 \end{bmatrix} \tag{22}$$

Now we let go $B \to 0$ considering that $n_j^{S^{(3)}} = -n_j^{S^{(2)}}$ and writing only S instead $S^{(2)}$ we get

$$J_1 = \lim_{B \to 0} \frac{1}{B} F_1 \tag{23}$$

$$J_1 = \int_\Gamma \left(w\delta_{j1}n_j^\Gamma - \sigma_{ij}n_j^\Gamma u_{i,1} \right) d\Gamma + \int_S \left(w\delta_{j1}n_j^S - \sigma_{ij}n_j^S u_{i,1} \right)_{,3} dS. \tag{24}$$

Considering further that the normal components $n_3^\Gamma = n_1^S = n_2^S = 0$ Eq. 24 becomes

$$J_1 = \int_\Gamma \left(wn_1^\Gamma - \sigma_{ij}n_j^\Gamma u_{i,1} \right) d\Gamma - \int_S \left(\sigma_{i3}u_{i,1} \right)_{,3} dS. \tag{25}$$

If we write all components we get

$$\begin{aligned} J_1 \ = \ & \int_\Gamma \left(wn_1^\Gamma \right) d\Gamma \\ & - \int_\Gamma \left[\left(\sigma_{11}n_1^\Gamma + \sigma_{12}n_2^\Gamma \right) u_{1,1} \right] d\Gamma \\ & - \int_\Gamma \left[\left(\sigma_{21}n_1^\Gamma + \sigma_{22}n_2^\Gamma \right) u_{2,1} \right] d\Gamma \\ & - \int_\Gamma \left[\left(\sigma_{31}n_1^\Gamma + \sigma_{32}n_2^\Gamma \right) u_{3,1} \right] d\Gamma \\ & - \int_S \left(\sigma_{13}u_{1,1} + \sigma_{23}u_{2,1} + \sigma_{33}u_{3,1} \right)_{,3} dS. \end{aligned} \tag{26}$$

If we take advantage of

$$\int_\Gamma wn_1^\Gamma d\Gamma = \int_\Gamma wd\Gamma_2, \quad \int_\Gamma wn_2^\Gamma d\Gamma = \int_\Gamma -wd\Gamma_1, \tag{27}$$

whereas $d\Gamma_1$ and $d\Gamma_2$ are the 1- and 2-component of the path increment $d\Gamma$, we get:

$$
\begin{aligned}
J_1 & = \int_\Gamma w \, d\Gamma_2 \\
& \quad - \int_\Gamma \left(\sigma_{11} u_{1,1} + \sigma_{21} u_{2,1} + \sigma_{31} u_{3,1} \right) d\Gamma_2 \\
& \quad - \int_\Gamma \left(\sigma_{12} u_{1,1} + \sigma_{22} u_{2,1} + \sigma_{32} u_{3,1} \right) d\Gamma_1 \\
& \quad - \int_S \left(\sigma_{13} u_{1,1} + \sigma_{23} u_{2,1} + \sigma_{33} u_{3,1} \right)_{,3} dA.
\end{aligned} \tag{28}
$$

Eq. (28) needs to be extended if thermal strain fields, volumetric loads like gravity and traction loads on the crack faces have to be considered.

$$
J_1 = J_1^{mech} + J_1^{th} - J_1^{bf} - J_1^{cf} \tag{29}
$$

$$
J_1^{th} = \int_{A(\Gamma)} \sigma_{ij} \varepsilon_{ij,1}^{th} \, dA \tag{30}
$$

$$
J_1^{bf} = \int_{A(\Gamma)} f_i u_{i,1} \, dA \tag{31}
$$

$$
J_1^{cf} = \int_{\Gamma^{(cf)}} t_i u_{i,1} \, d\Gamma^{(cf)} \tag{32}
$$

J_1^{mech} is the classical mechanical part and equivalent to Eq. (26) and (28), J_1^{th} is the correction for thermal strains, J_1^{bf} is the correction for body forces or volumetric loads and J_1^{cf} considers the crack face traction loads. $A(\Gamma)$ is the cross section area of the cylinder bounded by circumferential path Γ and $\Gamma^{(cf)}$ is the path segment along the upper and lower crack face. If we assume an isotropic thermal expansion coefficient α and only pressure loads p on the crack faces then we can simplify:

$$
J_1^{th} = \int_{A(\Gamma)} \left(\sigma_{11} + \sigma_{12} + \sigma_{13} \right) \varepsilon_{,1}^{th} \, dA, \tag{33}
$$

$$
J_1^{bf} = \int_{A(\Gamma)} \left(f_1 u_{1,1} + f_2 u_{2,1} + f_3 u_{3,1} \right) dA, \tag{34}
$$

$$
J_1^{cf} = \int_{\Gamma^{(cf)}} p u_{2,1} \, d\Gamma^{(cf)}. \tag{35}
$$

3.4   J-integral computation with ANSYS

We consider the following equation, which includes the correction terms for thermal fields, volumetric loads and crack face traction loads:

$$
\begin{aligned}
J_1 \;=\; & \int_{\Gamma} (w\delta_{j1}n_j - \sigma_{ij}n_j u_{i,1})d\Gamma \\
& - \int_{A(\Gamma)} (\sigma_{ij}n_j u_{i,1})_{,3}\,dA(\Gamma) \\
& + \int_{A(\Gamma)} \sigma_{ij}\varepsilon_{ij,1}^{th}\,dA(\Gamma) \\
& - \int_{A(\Gamma)} f_i u_{i,1}\,dA(\Gamma) \\
& - \int_{\Gamma^{(cf)}} p u_{2,1}\,d\Gamma^{(cf)}
\end{aligned}
\tag{36}
$$

The value of J_1 is theoretically independent from path Γ as long this path starts on
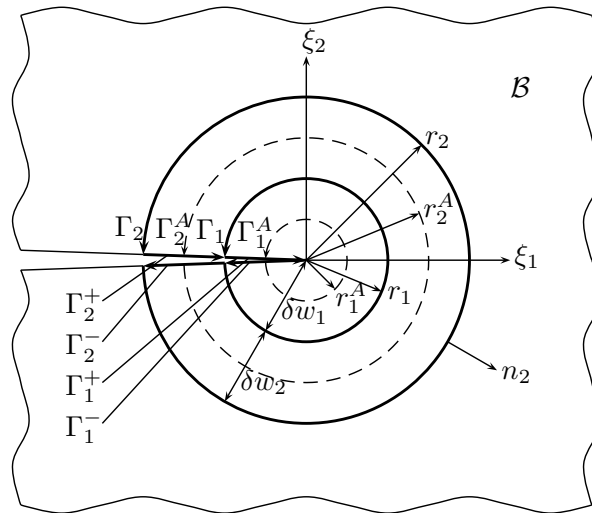
Figure 15: Integration scheme for two dimensional j-integral

a crack face, surrounds the crack tip and ends on the other crack face. If we consider plasticity J_1 becomes path dependent if the outer integration contour (surface) passes the plastic zone [5]. For small scale yielding a path independent integral can be computed in two dimensions if the integration path surrounds of the plastic zone. In three dimensions the integration boundary includes the top and bottom area $S^{(1)}$ and $S^{(2)}$ or $A(\Gamma)$ of the cylindric integration boundary, which always crosses the crack tip, where plasticity can occur. That is why a more or less significant path dependence will occur for three dimensional evaluations of J_1 when plasticity occurs. Therefore, we compute J_1 for several paths with increasing radius, to check if a saturation value of J_1 can be reached. Brocks and Schneider [5] suggest to take the highest calculated J_1 value with increasing domain size as the closest to the real far field J_1.

The different paths for the integral along Γ_l are concentric circles with increasing radii

$$
r_l = l\frac{r_m}{m} \quad \text{for} \quad l = 0 \dots m.
\tag{37}
$$

The paths necessary for the area integration over $A(\Gamma)$ have the radii

$$r_l^A = \frac{r_l + r_{l-1}}{2} \quad \text{for} \quad l = 1 \ldots m \tag{38}$$

and the corresponding width

$$\delta w_l = r_l - r_{l-1} \quad \text{for} \quad l = 1 \ldots m. \tag{39}$$

The area integration with ANSYS is then a summation over path integrals along Γ_l^A that are multiplied with their corresponding width.

$$
\begin{aligned}
J_1^m &= \int_{\Gamma_m} w n_1 d\Gamma_m \\
&- \int_{\Gamma_m} \sigma_{ij} n_j u_{i,1} d\Gamma_m \\
&- \sum_{l=1}^{m} \int_{\Gamma_l^A} (\sigma_{i3} u_{i,1})_{,3} d\Gamma_l^A \delta w_l \\
&+ \sum_{l=1}^{m} \int_{\Gamma_l^A} \sigma_{ii} \varepsilon_{,1}^{th} d\Gamma_l^A \delta w_l \\
&- \sum_{l=1}^{m} \int_{\Gamma_l^A} f_i u_{i,1} d\Gamma_l^A \delta w_l \\
&+ \sum_{l=1}^{m} \int_{\Gamma_l^+} p u_{2,1} d\Gamma_l^+ \delta w_l \\
&- \sum_{l=1}^{m} \int_{\Gamma_l^-} p u_{2,1} d\Gamma_l^- \delta w_l
\end{aligned}
\tag{40}
$$

Eq. (40) is computed with an ANSYS postprocessing tool, taking advantage of the powerful ANSYS path commands.

4   Results

The results requested by the benchmark are the variation of temperature, axial and hoop stress trough the RPV wall for the global model without a crack but at the position for the assumed crack. Furthermore, the variation of the stress intensity factors K_I as a function of the crack tip temperature for the deepest point of the crack and a position 2 mm below the cladding-base material interface are required. Then the maximum allowable critical temperatures for both positions shall be provided. Additionally, we present the variation of K_I along the crackfront for selected times.

4.1   Global model

The figures 16, 18 and 20 show data for a path across the RPV wall at the assumed crack position for different times. The figures 17, 19 and 21 show the same data but plotted over time for different wall coordinates. In this plots, surface means the inner RPV surface, a=2 mm is a point in the base material 2 mm away from the cladding-base material interface and a=15 mm is a point where the deepest point of the assumed crack would be located. To be clear, there is no crack in the global model.

In Fig. 16 the variation of temperature is plotted over the RPV wall coordinate. At the beginning of the simulation the RPV wall has a constant temperature of 267°C. With increasing time the temperature on the inner surface decreases. The temperature gradient reaches its maximum at 1000 seconds, which is the same time as the axial and hoop stress reach their maximum, as it can be seen in the figures 18 and 20. Due to the reduced thermal conductivity of the cladding material (see table 2), the temperature gradient is steeper in the cladding (0...9 mm) than in the base material. The temperatures in Fig. 17 show an expected run. The wall cool down is fastest at its inner surface.

The stresses in Fig. 19 and 21 show an interesting run. They decrease during the first 300 seconds due to pressure reduction by opening the PRZ SV. Then follows a quite fast increase, which is only caused by the thermal shock. After 1000 seconds the stresses are decreasing again as well as the temperature gradient. At 3600 seconds the PRZ SV is closed which causes a repressurization of the vessel and therefore an sudden increase of the stresses. It is worth mentioning that the hoop stress increase twice as much as the axial stress, which we expect in a cylindrical vessel. This is the reason why the assumed crack will be aligned in axial direction, so that the hoop stress causes the mode I crack opening.

For the stress plots of the surface point in the figures 19 and 21 a small drop of after 1000 seconds occurs. This is a numerical artefact, possible caused by a relocation of plastic zones. It appears only in the global model, where the aspect ratios of the cladding elements are bad.

The figures 18 and 20 show the variation of the stresses through the RPV wall. As expected the tensile stress values are maximal at the inner surface of the RPV. For times with low internal pressure compressive stresses are present in the wall. This and the increase of the stresses at the vessel outside is caused by the residual stresses in the weld lines.
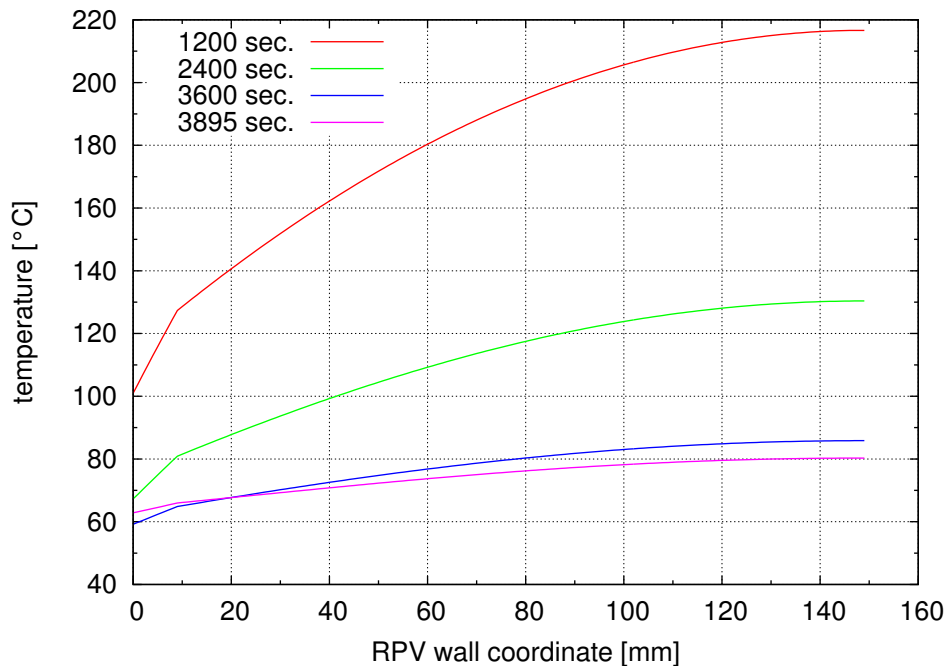
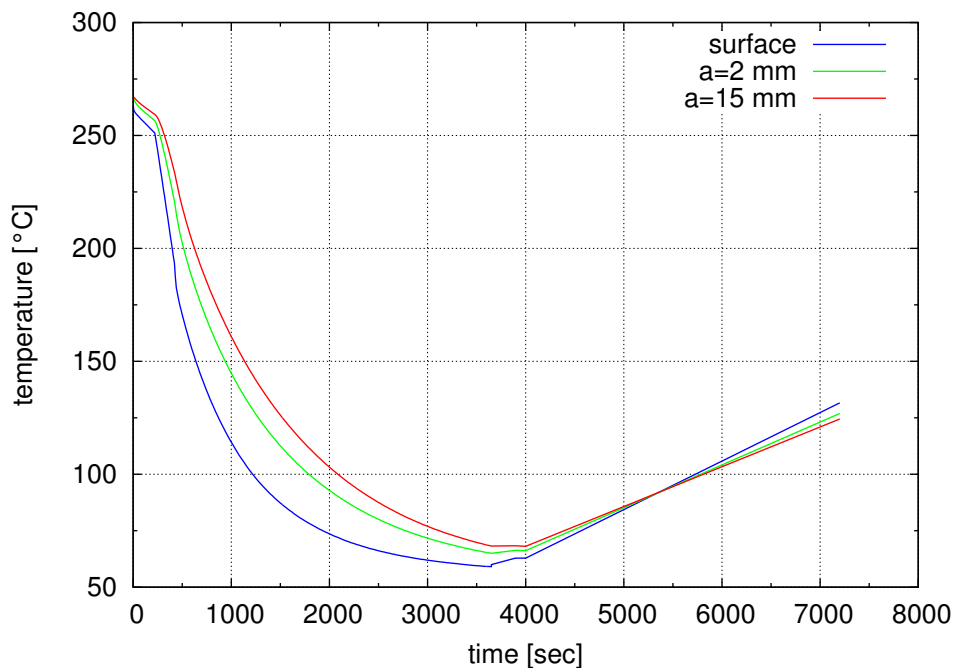**Figure 16:** Variation of temperature through the RPV wall thickness

Figure 17: Variation of temperature in time for different positions of the RPV wall, surface - inner surface, a=2 mm - a point 2 mm inside the base material, a=15 mm - assumed crack tip position
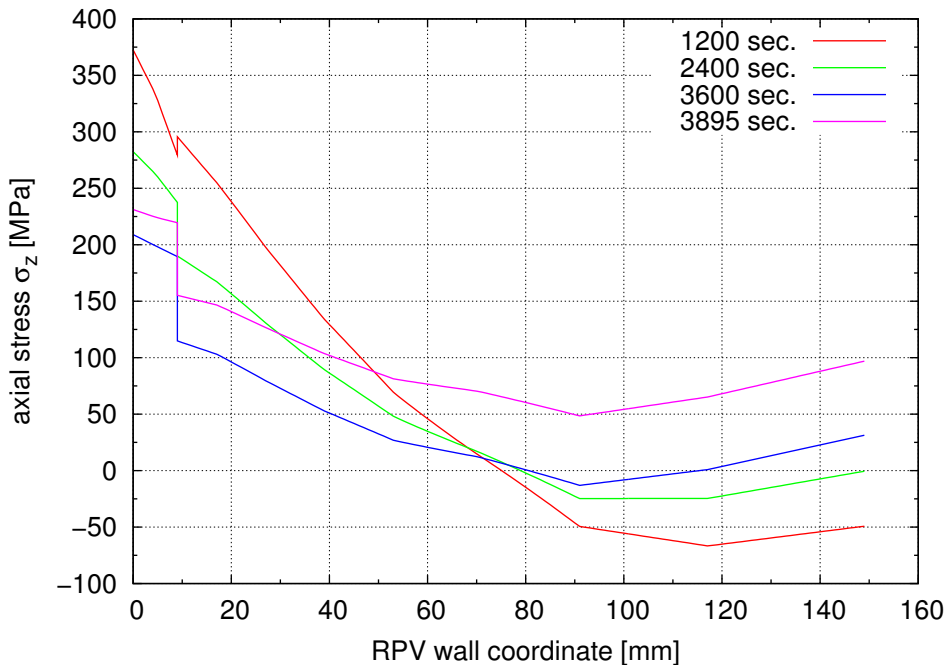
Figure 18: Variation of axial stress through the RPV wall thickness in the crack free region
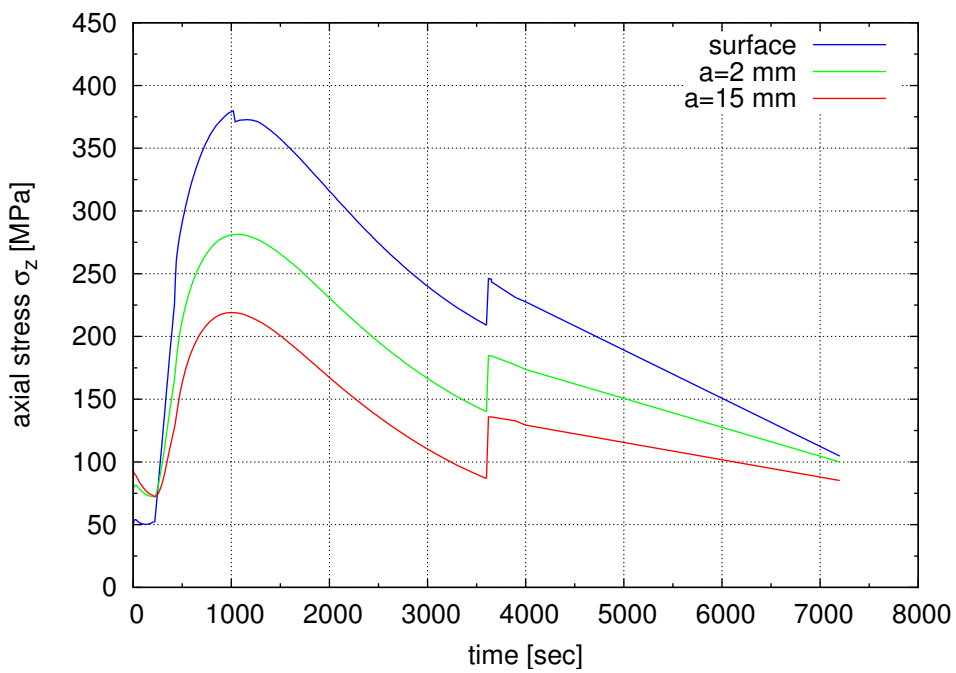

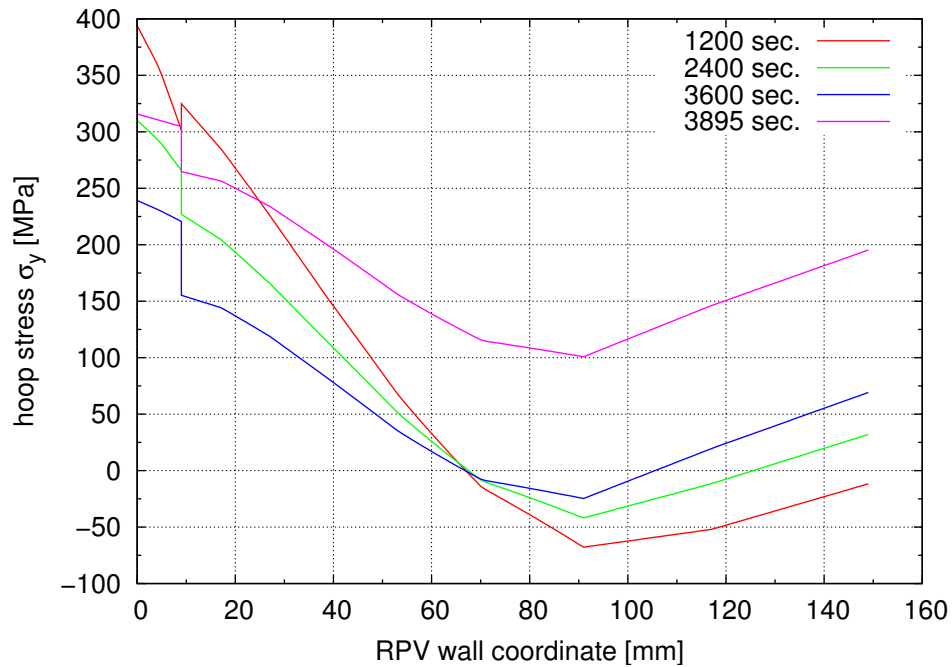**Figure 19:** Variation of axial stress in time for different positions of the RPV wall

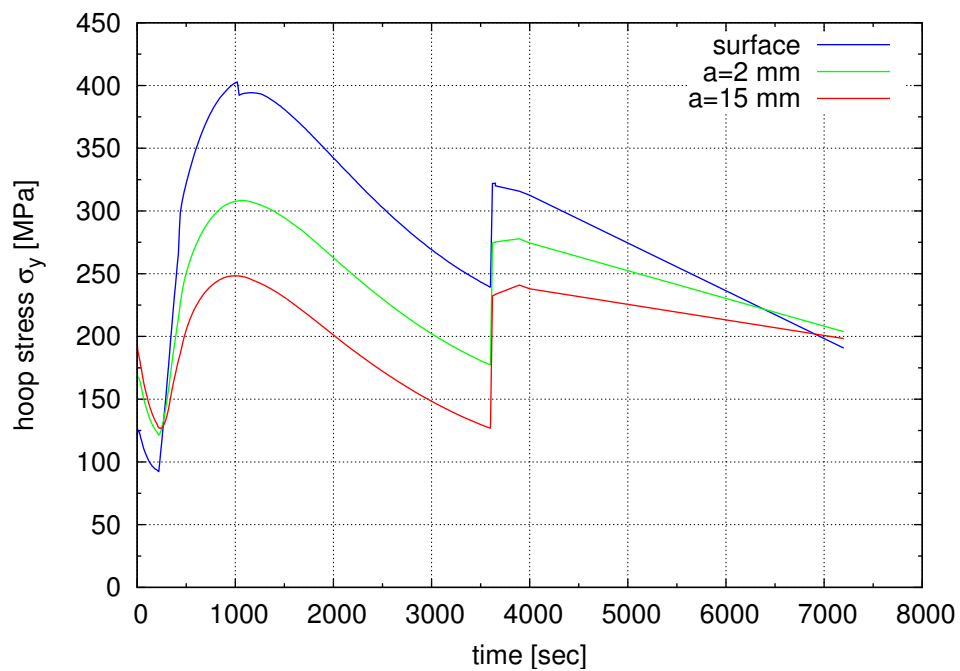**Figure 20:** Variation of hoop stress through the RPV wall thickness in the crack free region

Figure 21: Variation of hoop stress in time for different positions of the RPV wall

4.2 Underclad crack

Fig. 22 shows the variation of the stress intensity factor K_I computed with the j-integral technique for the deepest point of the crack (a=15 mm) and a point (a=2 mm) below the cladding-base material interface. The point at a=2 mm is located outside of the weld. Therefore it was assumed, that in this location there are no residual stresses. Contrary to that, the VERLIFE code suggests that all points of the crack front are supposed to lie entirely in the weld. The principal course is the same as for the hoop stress (see Fig. 21), with a slightly decrease at the beginning due to the pressure reduction, then an increase up to the maximum at 1000 seconds due to the thermal shock effects. It follows a decrease again, as the temperature gradient through the vessel wall decreases. The repressurization is the critical phase for this scenario, a sudden increase of K_I must be noted. The variation of K_I along the crack front is shown in Fig. 22. The maximum of K_I is found at an angular position of $\alpha = 90°$. The effect of the residual stresses in the weld lines, which cause an increase of K_I between 60° and 120°, can clearly be seen.

In Fig. 24 is K_I plotted as a function of the crack tip temperature together with the $[K_{IC}]_3$-curve with a value for T_k^a chosen as

$$T_k^a = \min \left(T - \frac{\ln \frac{K_I - 26}{36}}{0.02} \right) \tag{41}$$

for all computed pairs of K_I and T. It is obvious that the repressurization causes the critical $K_I = 40.2$ MPam$^{0.5}$ at a crack tip temperature $T = 68.9°$C. The maximum value of $K_I = 43$ MPam$^{0.5}$ occurs at 1000 seconds where the crack tip temperature is $T = 170°$C, which is an uncritical state.
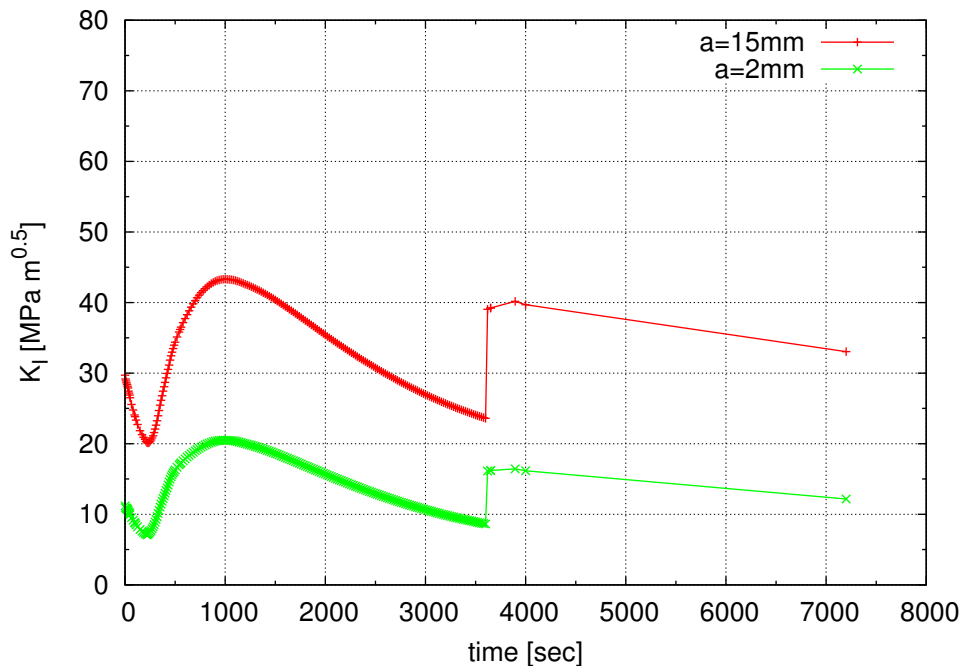

Figure 22: Variation of the stress intensity factor value K_I as a function of time for different positions at the crack front
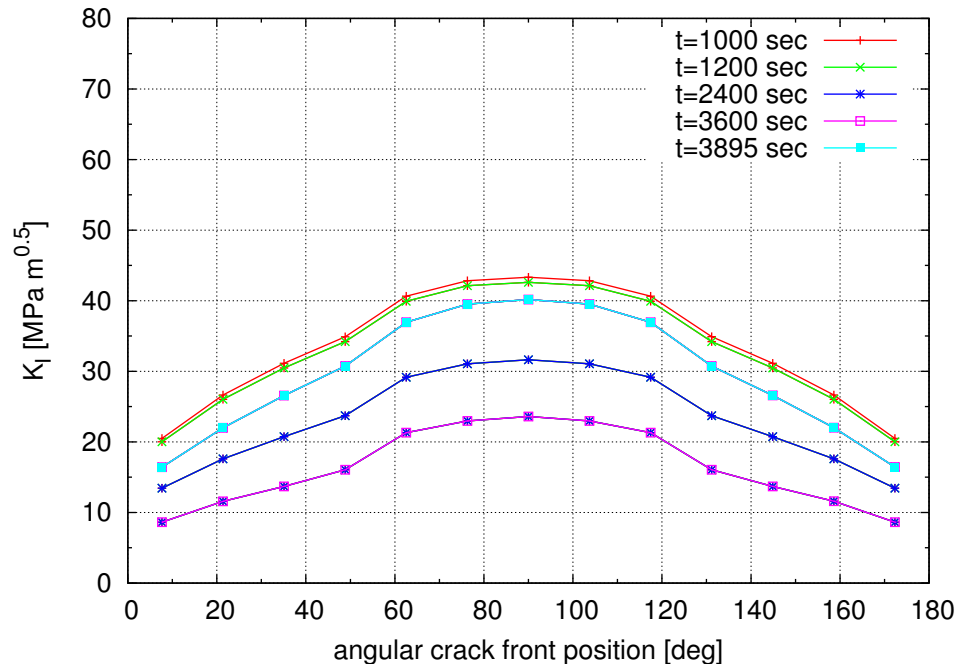
Figure 23: Variation of the stress intensity factor value K_I along the underclad crack front for different times
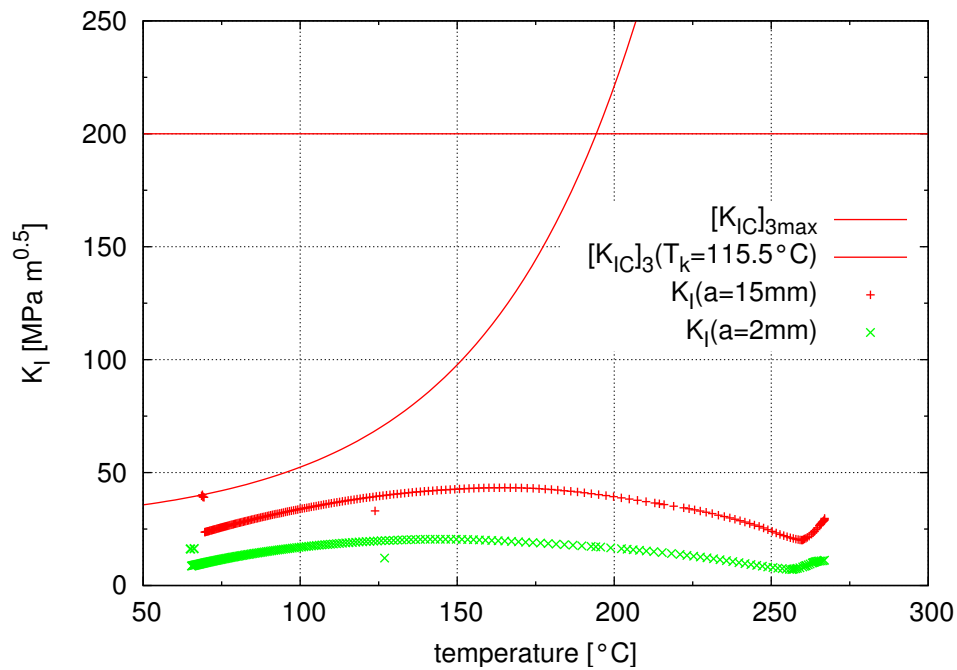

Figure 24: Stress intensity factor value K_I as a function of temperature and $[K_{IC}]_3$ curve for the maximum allowable transition temperature $T_k^{a=15mm} = 115.5°\mathrm{C}$

4.3   Surface crack

The results for the surface crack are in principle the same as for the underclad crack, but with elevated values of the stress intensity factors. Here also, the repressurization of the RPV causes the critical value of $K_I = 67\,\mathrm{MPam}^{0.5}$ at a crack tip temperature of $T = 68.9°\mathrm{C}$.
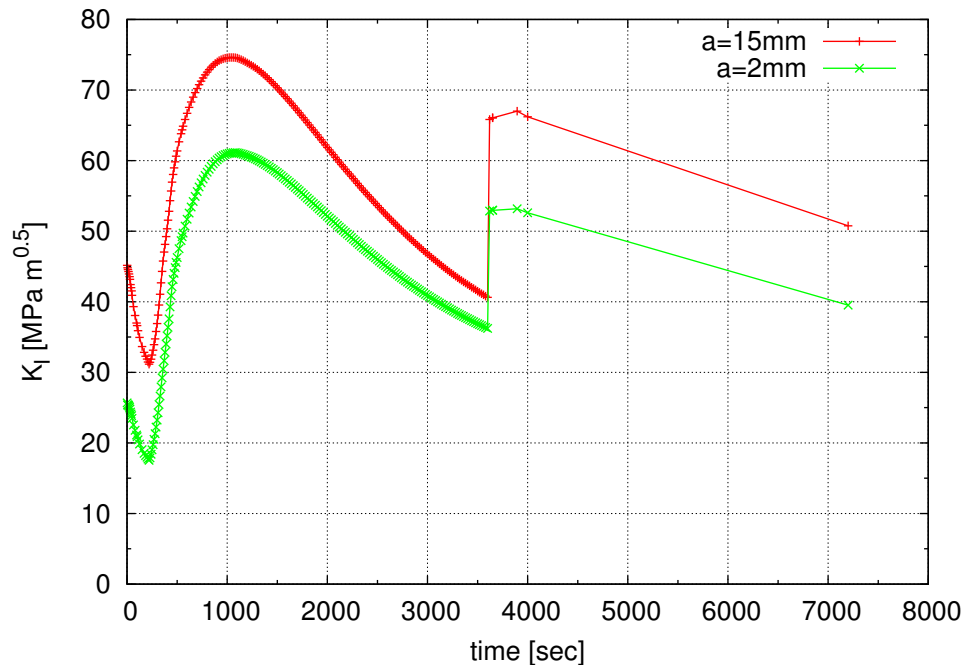

Figure 25: Variation of the stress intensity factor value K_I as a function of time for different positions at the crack front
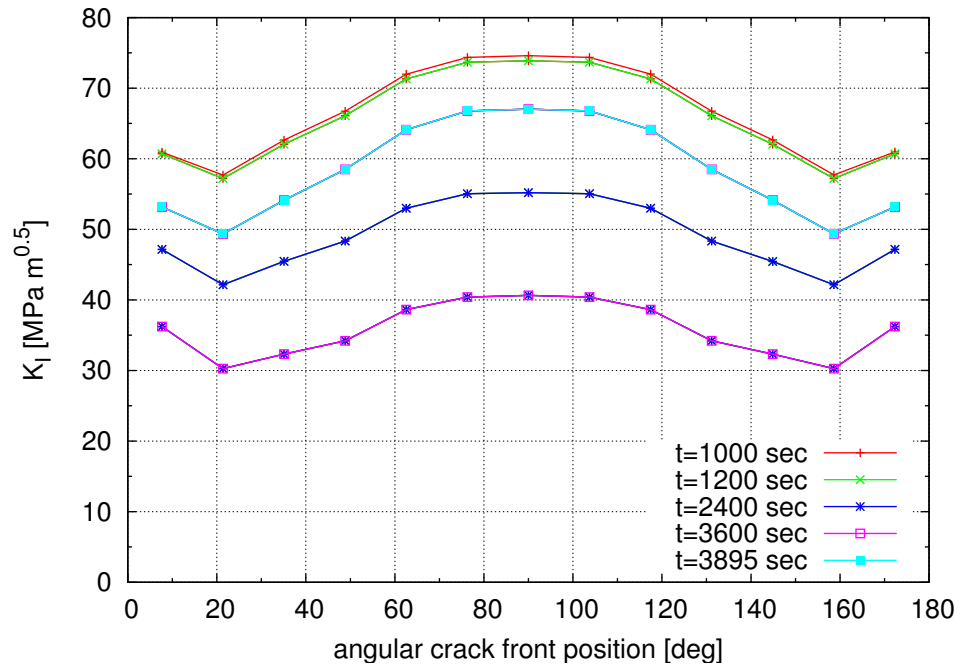
Figure 26: Variation of the stress intensity factor value K_I along the surface crack front for different times
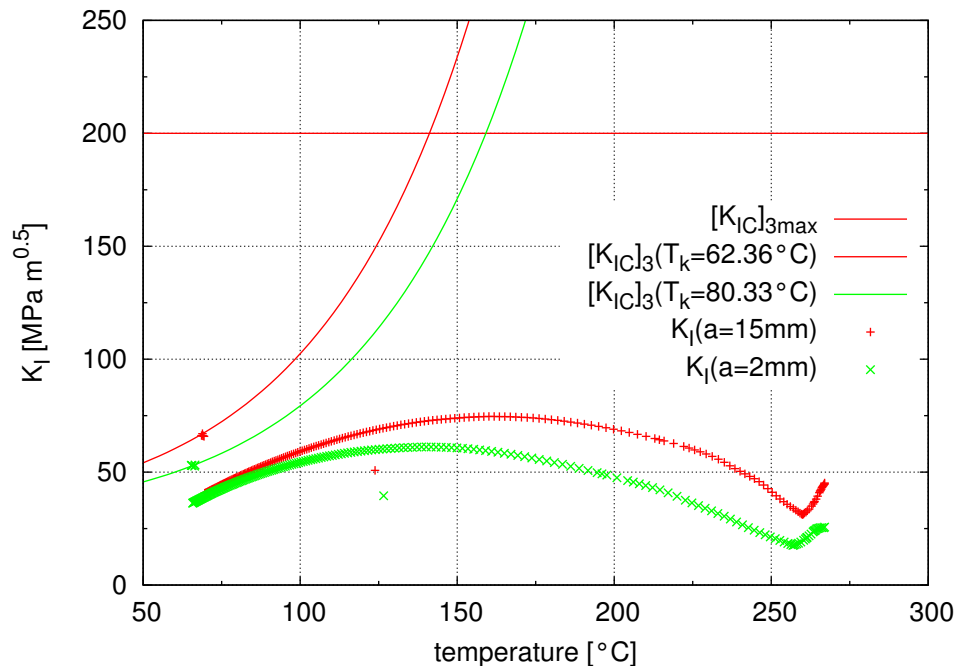

Figure 27: Stress intensity factor value K_I as a function of temperature and $[K_{IC}]_3$ curve for the maximum allowable transition temperature $T_k^{a=15mm} = 62.36°$C, $T_k^{a=2mm} = 80.33°$C

5   Conclusions and Discussion

Table 6 shows the main results of this work, as there are the critical $K_I(T)$ and T_k^a values for the underclad and the surface crack located in the most embrittled weld line of a WWER-440 RPV during a thermal shock emergency scenario. For comparison additional values are given which are obtained using simplified approaches, as there are the kcalc procedure of ANSYS [2] and the VERLIFE engineering approach. Both methods are not qualified since they are valid only for elastic cases and the VERLIFE simplified engineering approach does not take into account an existence of a cladding.

For small scale yielding at the crack tip, as it is in this case, the kcalc approach delivers conservative K_I and T_k^a values, since it uses the normal displacements of the crack faces and the elastic properties of the material to compute K_I. These displacements are larger if plasticity occurs.

The VERLIFE simplified engineering approach uses the stress components normal to the crack face for K_I computation. These stresses are limited if plasticity occurs. Furthermore there are restrictions to the crack geometry. As the results in table 6 show this approach delivers a strongly conservative value for the underclad crack. For the surface crack the K_I value is only slightly conservative, compared to the one obtained with the j-integral method.

Reliable values are obtained by the j-integral method even for small scale yielding at the crack tip.

Up to here, the VERLIFE procedure is clear within the recommendations of the methods. A more critical point concerns the finite element crack modelling for the underclad crack. The VERLIFE code allows to assume an underclad crack, if the fracture properties of the austenitic cladding are known and if the cladding integrity is assured. As mentioned in section 3.1 the common nodes of cladding and base material cause an artificial crack mouth clamping, which results in an underestimation of K_I for an underclad crack. A better approach might be to define a crack which affects both cladding and base material, as shown in Fig. 28. The postulation of a surface crack leads to more conservative results.

Table 6: Maximum allowable transition temperatures T_k^a along with the K_I^a and crack tip temperature T values for the deepest point (a=15mm) calculated with different methods

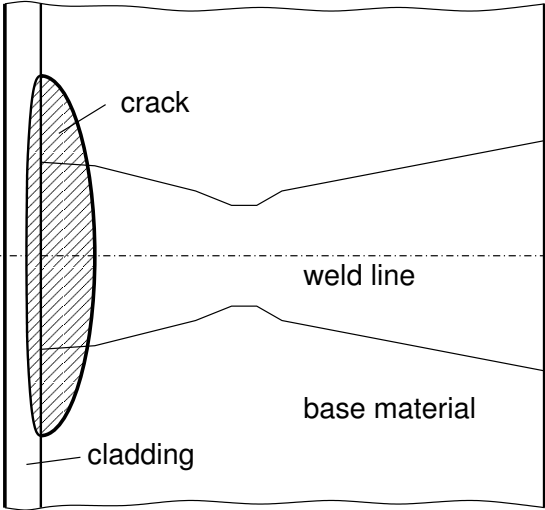|		underclad crack			surface crack		
		j-integral	kcalc	verlife	**j-integral**	kcalc	verlife
T	[°C]	**68.9**	68.9	68.9	**68.9**	68.9	68.9
K_I^a	[MPam$^{0.5}$]	**40.2**	42.9	53.8	**67.0**	68.5	67.6
T_k^a	[°C]	**115.5**	106.1	81.8	**62.4**	60.0	61.7

Figure 28: Crack affecting both cladding and base material

References

[1] Eurotom Call 2004. VVER safety research. Technical report, Sixth Framework Programme Euratom, Other Activities in the Field of Nulcear Technologies and Safety, 2005.

[2] ANSYS 10.0. *ANSYS 10.0 Documentation*, 2005.

[3] B.R. Bass, R.H. Bryan, J.W. Bryson, and J.G. Merkle. Applications of energy-release-rate techniques to part-trough cracks in experimental pressure vessel. *Journal of Pressure Vessel Technology*, 104(4):308–316, 1982.

[4] B.R. Bass and J.W. Bryson. Energy release rate techniques for combined thermo-mechanical loading. *International Journal of Fracture*, 104(1):R3–R7, 1983.

[5] W. Brocks and I. Schneider. Numerical aspects of the path-dependence of the j-integral in incremental plasticity. internal report GKSS/WMS/01/08, GKSS-Forschungszentrum Geesthacht, 2001.

[6] M. Brumovsky. Unified procedure for lifetime assessment of components and piping in WWER NPPs VERLIFE. Technical report, European Commision, 5th Euratom framework programme 1998–2002, 2003.

[7] C.P. Cherepanov. Crack propagation in continous media. *Journal of Applied Mathematics and Mechanics*, 31(3):476–488, 1967.

[8] J.D. Eshelby. The continuum theory of lattice defects. *Solid State Physics*, 3:79–114, 1965.

[9] M. Kikuchi, H. Miyamoto, and Y. Sakaguchi. Evaluation of three-dimensional j-integral of semielliptical surface crack in pressure vessel. In *SMIRT 5, G7/2*, 1979.

[10] V. Pistora and P. Kral. Evaluation of pressurized thermal shocks for VVER-440/213 reactor pressure vessel in NPP dukovany. In *Transactions of 17th International Conference on Structural Mechanics in Reactor Technology (SMIRT 17), Paper No. G01-3*, 2003.

[11] J.R. Rice. A path-independent integral and the approximate solution of strain concentration by notches and cracks. *Journal of Applied Mechanics*, 35:379–386, 1968.

[12] C.F. Shih, B. Moran, and T. Nakamura. Energy release rate along a three-dimensional crack front in a thermally stressed body. *International Journal of Fracture*, 30:79–102, 1986.

[13] J. Sievers and A. Höfler. Application of the j-integral concept to thermal shock loadings. *Nuclear Engineering and Design*, 96:287–295, 1986.